# Nanoparticle Growth in Thermally Diffusive Sublimation-Condensation Systems with Low Vapor Pressure Solids

Li Li<sup>1</sup>, Ke'La A. Kimble<sup>2</sup>, Brock A. Mitts<sup>2</sup>, Michelle Heilig<sup>1</sup>, Yuechen Qiao<sup>1</sup>, Jihyeon Lee<sup>1</sup>, Kimberly A. Prather<sup>2,3</sup> & Christopher J. Hogan Jr. <sup>1\*</sup>

<sup>1</sup>Department of Mechanical Engineering, University of Minnesota, Minneapolis, MN USA

<sup>2</sup> Department of Chemistry & Biochemistry, University of California, San Diego

<sup>3</sup>Scripps Institute of Oceanography, University of California, San Diego

#### **Submitted to:**

# **Journal of Aerosol Science**

\*To whom correspondence should be addressed: <a href="https://hogan108@umn.edu">hogan108@umn.edu</a>

#### **Abstract**

Engineered, condensational growth of aerosol particles is a well-established technique incorporated into particle detection and sampling systems. It is typically accomplished through passage of particles through controlled temperature, supersaturated systems with moderate-to-high vapor pressure compounds, which are liquid at room temperature. However, there are instances where it is advantageous to intentionally grow particles with room temperature, low vapor pressure (<10<sup>-3</sup> Pa) solid compounds, either as part of particle collection or ionization systems. Sublimationcondensation, though demonstrated previously, is much less examined, particularly for nanoparticle growth. In this study, we examine a thermally diffusive, laminar flow sublimationcondensation system, wherein solid organic powders (all ionization facilitating matrices) are sublimated at moderate temperature (70-130°C) and subsequent cooling results in vapor supersaturation, promoting growth of particles. The extent of particle growth was characterized via tandem differential mobility analyzer (TDMA) measurements, with 30 nm-200 nm particles. The grown diameter distributions were monitored for three different low vapor pressure organic solids at variable sublimator temperature settings. We found optimized operating conditions enabled particle growth always above diameters of 500 nm. Growth experiments with 7 nm protein (transferrin) particles using ferulic acid as the working solid additionally yielded grown particles in excess of 200 nm in diameter. However, we also found heterogeneous growth occurred simultaneously with homogeneous nucleation of the working solid, which could not be avoided if growth to diameters > 500 nm was desired. Homogeneously nucleated particles were broadly distributed in size, and generally smaller than the test particles grown by condensation, but still with diameters in excess of 100 nm. While SEM images of grown particles revealed smooth surfaces not indicative of agglomeration of homogeneously nucleated particles, we cannot rule out the contribution to growth of homogeneously nucleated particle coagulation with sampled particles in the growth system. By comparing to numerical simulations, we use TDMA measurements to estimate effective vapor pressures for the tested sublimated solids, assuming growth occurred solely by vapor condensation. Simulations suggest that saturation ratios in excess of  $10^2$  are needed for nanoparticle growth.

#### 1. Introduction

Challenges in detecting, sampling, and chemically analyzing aerosol nanoparticles are frequently overcome through instruments where such particles are grown to submicrometer and supermicrometer sizes via controlled condensation of a room temperature liquid (working fluid) onto particles. This is accomplished frequently in flow tube systems, wherein supersaturation of the working fluid is created through controlling and modulating temperature and vapor concentration profiles. Controlled condensation along these lines is exploited in condensation particle counters (Agarwal & Sem, 1980; Bricard et al., 1976; McMurry, 2000), virtual impactionbased aerosol concentrators (Kim et al., 2001), and techniques to increase particle charge levels (Kreisberg et al., 2018; Suh et al., 2005), among others. The majority of "engineered" condensation systems for aerosol analysis utilize working fluids of moderate-to-high vapor pressure at room temperature, only requiring slight temperature elevation (~15-20 K) to drastically increase vapor number concentration and drive sufficient supersaturation for growth. Overwhelmingly water (Hering et al., 2005) and n-butanol (Agarwal & Sem, 1980; Stolzenburg & McMurry, 1991) are used as working fluids, but diethylene glycol (Jiang et al., 2011; Rörup et al., 2022), dibutyl phthalate (Gamero-Castaño & Fernández de la Mora, 2000; Okuyama et al., 1984), and a variety of others (Iida et al., 2009) have been applied, typically in an effort to demonstrate condensational growth onto increasingly smaller particles.

In expanding aerosol analysis systems, there are instances where it is advantageous to collisionally grow low vapor pressure (at room temperature) solid materials. For example, with typical condensation systems, following condensation, evaporation can occur if the system is not conditioned to prevent evaporation. With low vapor pressure materials, evaporation of grown particles is much less of a concern on the timescale of aerosol measurement or sampling systems

(i.e. timescales of seconds to minutes). Growth with low vapor pressure solids may also be desirable to avoid dissolution or chemical reaction between particles and their surroundings (Post et al., 2018), or perhaps more directly, towards facilitating specific chemical interactions between particles and the condensing compound. For example, growth with an ionization-facilitating matrix is a necessary step in in-flight matrix assisted laser desorption ionization (MALDI) of aerosol particles (Fei et al., 1996; Jackson et al., 2004; Jackson & Murray, 2002; McJimpsey et al., 2008).

However, sublimation-condensation with low vapor pressure solids, as a means to grow particles under 200 nm in diameter, is much less studied for aerosols, and presents some distinct challenges from working fluid condensation. First, for most solids where the vapor pressure is negligibly low at room temperature, the vapor pressure has only been estimated, or may not be known. This complicates *a priori* system design. Second, for low vapor pressure systems, significantly higher saturation ratios may be required to promote condensational growth, as the condensation growth rate depends upon the vapor number density (Friedlander, 2000). Creating higher levels of supersaturation may also promote homogeneous nucleation of particles alongside condensation. This in turn may lead to coagulation growth both of purely nucleated particles, and of sampled particles with homogeneously nucleated particles, as has been demonstrated for growth schemes with noble metal vapors (Boies et al., 2011).

In the present study, we examine the capabilities of a laminar flow, thermally diffusive sublimation-condensation system to collisionally grow low vapor pressure, room temperature solid organic compounds onto nanoparticles. The sublimation-condensation system applied here functions similar to the condensation system in condensation particle counters (Agarwal & Sem, 1980), and Sinclair-LaMer aerosol generators (Perry & Smaldone, 1985; Sinclair & La Mer, 1949),

but with a solid powder (working solid) instead of a working fluid. As working solids, we specifically focus on three ionization-facilitating matrix materials which are utilized frequently in matrix assisted laser desorption ionization-mass spectrometry (MALDI-MS). This focus is largely driven by interest in advancing online MALDI-MS for aerosol particles, as can be accomplished with matrix -coated particles entering an aerosol time-of-flight mass spectrometer (ATOFMS). Aerosol MALDI-MS has potential applications in the real-time analysis of organic aerosols and bioaerosols at the single particle level (Stowers et al., 2000; van Wuijckhuijse et al., 2005). Importantly, aerosol MALDI-MS has been demonstrated in a number of prior studies precisely in which matrix materials were grown onto particles (Fei et al., 1996; Harris et al., 2005, 2006; Jackson et al., 2004; Jackson & Murray, 2002; Stowers et al., 2000; van Wuijckhuijse et al., 2005; Xia et al., 2010; Zhou et al., 2006). Specific proof-of-concept demonstration of matrix material condensation with atmospheric pressure, laminar flow systems is provided in Harris et al (Harris et al., 2005, 2006), Jackson and Murray (2002), Jackson et al. (2004), and Stowers et al. (2000). However, in these prior works, because of the focus on collecting mass spectrometric data, data on the sublimation-condensation system capabilities in terms of particle growth, sensitivity to operating temperatures, extent of homogeneous nucleation, potential contributions of coagulational growth, and application to sub 200 nm particles were not provided. We believe there is thus still a need for fundamental studies of low vapor pressure matrix material growth onto nanoparticles to understand the potential capabilities of sublimation-condensation in aerosol sampling, detection, and analysis.

The subsequent sections describe the design of the sublimation-condensation system, testing the extent of condensational growth via tandem differential mobility analyzer (TDMA)(Rader & McMurry, 1986) measurements, simulation of the sublimation-condensation

process, and evaluation of the extent of homogeneous nucleation in the system. The data presented show the extent of particle growth for three different materials, and through fitting simulation results to experiments, we provide estimates of the effective Clausius-Clapeyron equation parameters (vapor pressure parameters) for the three tested working solids if growth was solely attributable to condensation.

#### 2. Experimental and Numerical Methods

Sublimation-Condensation System Description

The designed sublimation-condensation system is depicted in Figure 1a. This figure includes an isometric view of the device and a photograph as an inset. As noted in the introduction, the design is based on approaches commonly employed for laminar flow, thermally diffusive, condensation particle counter systems (Agarwal & Sem, 1980), and more specifically it is similar to the system developed by Attoui (2021) to generate singly-charged particles from low vapor pressure materials. Aerosols enter the sublimation region (13.4 cm in length) at a flow rate of 0.3 SLM (standard liters per minute); the entire sublimation-condensation system has a particle residence time of 23.31±1.66 s, based on particle trajectory calculations presented subsequently. A bed of the working solid powder is placed evenly throughout both the sublimation and the condensation region. Heating tape (BriskHeat, Columbus, OH, USA) is wrapped around the sublimation tube, held at 70-130°C (higher than the 40°-50° C used in water and n-butanol systems (Hering et al., 2005; Stolzenburg & McMurry, 1991)), facilitating sublimation of the working solid and leading to nearly vapor-saturated flow exiting the sublimator. We examined the performance with three distinct working solids: ferulic acid (FA, Nature & Nurture USA), 2,4dihydroxybenzoic acid (DHB, Sigma-Aldrich, Saint Louis, MO, USA)

bis(tetramethylguanidino)naphthalene (TMGN, Sigma-Aldrich, Saint Louis, MO, USA), a more recently developed ionizable matrix (Cao et al., 2011)). These three materials were selected based upon prevalent use in MALDI-MS, having melting temperatures < 250 °C, and minimal toxicity which is certainly of concern for in-flight particle growth as the working solid is introduced into the vapor phase. An insulating piece of polytetrafluoroethylene (PTFE) is placed between the sublimator and condenser. The temperature of the condenser is maintained at ~10 °C using a counter-current, water cooled, heat exchanger, with an aquarium water pump used to recirculate water from an ice bath around the condenser. As the aerosol flow exits the sublimator and is cooled by the condenser, supersaturation of the vapor results, as heat transfer to the walls occurs more rapidly than mass transfer (Le, the Lewis number, is greater than unity) (Thomas et al., 2018) for high molecular weight vapor molecules in air. Supersaturation leads to condensation of the working solid onto particles present in the flow, but may also lead to homogeneous nucleation of the solid material, particularly at higher sublimator temperatures. As part of system validation (with subsequent comparison to simulations), the temperature profile along the centerline of the flow within the sublimation-condensation system was measured using a K-type thermocouple for nominal heating temperatures of 70, 80 and 90°C, at 2.54 cm axial distance increments (13 measurements in total, spanning the sublimator and condenser).

#### Particle Growth Measurements

A schematic diagram of the TDMA system used for evaluating particle growth with the sublimation-condensation system is shown in Figure 1(b). Particles ranging from 10 nm to 200 nm were generated with a custom made, constant output pneumatic atomizer, operated with a backing air pressure of 138 kPa and atomizing a 0.3 wt % potassium chloride (KCl) aqueous solution. The

atomizer output flow was split, and 0.3 SLM was dried by a silica-bead diffusion drier and subsequently directed into a 85Kr bipolar charger (10mCi, Age 10.05yr, 5.32mCi at the time measurement conducted) to bring particles to a near steady-state charge distribution. Following drying (bringing the relative humidity to < 10%) and aerosol charging, the flow entered a DMA (Knutson & Whitby, 1975) (custom made, but with dimensions identical to the TSI Inc. model 3081 long DMA). The DMA was operated with a recirculating sheath flow of 3.0 SLM of air. A fixed, negative voltage was applied to this DMA to select particles of a target mobility and hence target mobility diameter (of positive charge state). While the first DMA primarily transmitted singly charged particles, it is important to note above ~100 nm in mobility diameter, a combination of singly charged, doubly charged, and higher charge state particles were transmitted through the DMA (Johnson et al., 2020). However, singly and doubly charged particles could later be distinguished from one another after remeasurement following growth. The nearly monodisperse aerosol particles exiting from the first DMA passed into the sublimation-condensation system where they interacted with supersaturated working solid vapor, facilitating their growth. Particles then passed into a second DMA (without passage through a bipolar ionization source). The second DMA applied voltage was stepped at 299 V from 20 V to 9000V (holding each voltage for 3 s in measurement, with a delay time of 3 s between measurements), while its sheath flow was operated at 3.0 SLM. Particles that transmitted through the second DMA were detected via a condensation particle counter (CPC, TSI Model 3776 C).

In addition to experiments with salt particles, to examine the lower size limit of the sublimation-condensation system, condensational growth of FA onto transferrin (Sigma-Aldrich, Saint Louis, MO, USA), a nominally 7 nm diameter protein (Lee et al., 2022), was examined. For these experiments, an aqueous transferrin solution at a concentration of 30 µg mL<sup>-1</sup> was aerosolized

using a commercial aerosol generator (Kanomax Nano Aerosol Generator (NAG) Model 3250) (Jeon et al., 2016), dried via a diffusion silica-bead drier, and passed through a Po-210 bipolar ion source at a flow rate of 1.5 SLM. A nanoDMA (TSI Model 3085) was then used to isolate transferrin monomers, which were directed into the sublimation-condensation system, operated with FA at 90° C. The resulting size distributions were then measured with a second DMA and CPC as in experiments with >30 nm mobility diameter particles noted above.

All tandem DMA measurements resulted in measured CPC signal as a function of applied second DMA voltage, for a prescribed first DMA selected mobility for each working solid material tested. To quantify growth, these data were converted to a size distribution function  $(dN/dln(d_p))$ , the number concentration per unit natural log change in diameter) following the simplified procedure in Qiao et al. (2022), however excluding the charge distribution correction, as all particles exiting the first DMA were charged. While the inversion procedure applied does not correct for multiply charged and approximates the DMA transfer function as triangular (Knutson & Whitby, 1975), we note that we are not concerned with evaluating quantitatively particle number concentrations from DMA measurements and more concerned with monitoring the extent of particle growth with clear diameter shifts in excess of 10 nm, for which this inversion procedure is satisfactory.

Finally, to examine the morphology of the particles after growth, we collected particles with the first DMA set to maximally transmitted singly charged 102 nm particles, TGMN as the working solid, and sublimator settings at 80° C and 90° C, respectively. The second DMA was set to maximally transmit 531 nm particles at 80° C and 758 nm particles at 90° C in diameter accordingly. Collection was carried out for 1-5 minutes using a Nanometer Aerosol Sampler (TSI model 3089, (Dixkens & Fissan, 1999)). Collection was also carried out bypassing the

sublimation-condensation system and second DMA for reference. Particles were imaged using a Hitachi SU-8230 scanning electron microscope (SEM) at the University of Minnesota Characterization Facility.

## Homogenous Nucleation Measurement

The tandem DMA approach is "blind" to homogenously nucleated particles because of the lack of bipolar charging performed after passage through the sublimation-condensation system; homogeneously nucleated particles are neutral in charge state (note also ions cannot pass through the first DMA in TDMA experiments as they are too high in electrical mobility) and are not transmitted through DMAs without charge conditioning. To examine the extent of homogeneous nucleation in the sublimation-condensation system, as shown in Figure 1c, a flow of HEPA-filtered room air at 0.3 SLM was directly passed to the sublimation-condensation system. Any nucleated particles were then brought into a <sup>85</sup>Kr bipolar charger followed by a single DMA and CPC. Stepping the voltage in the DMA in an identical fashion to the second DMA in tandem DMA measurements, we determined mobility distributions of homogeneously nucleated particles, using the same data inversion procedure for tandem DMA measurements, but also correcting for the fraction of singly charged particles (using the charge distribution from Li and Gopalakrishnan (2021) and Suresh et al(2021)). The sublimation region was set to temperatures ranging from 70-100°C for homogeneous nucleation measurements.

#### Numerical Simulations

A combined fluid flow, heat transfer, and mass transfer model was used to examine temperature and normalized working solid vapor concentration profile in the system (Hao et al.,

2021). These simulation results were subsequently used for particle growth modeling wherein particle trajectories were tracked via a Brownian Dynamics algorithm and allowed to change size via condensation (Gopalakrishnan & Hogan, 2011) (or evaporation) based on the temperature and saturation ratio of the local conditions. Details of simulations and validation by comparing results to traditional Graetz theory are both provided in the supporting information (including Figure S1 for Graetz theory comparison of centerline temperature vapor pressure, saturation ratio, and saturation vapor pressure profiles). Unfortunately, the saturation vapor pressures of the working solids are not known. Therefore, we used experimental measurements to fit Clausius-Clapeyron saturation vapor pressure curves to data. The fitting procedure is also described in the supporting information and was used to convert normalized working solid vapor concentration profiles to saturation ratio profiles, enabling prediction of particle growth. Importantly, in the fitting procedure we assumed that growth is entirely due to condensation of the working solid, without substantial contribution from coagulational growth by homogeneously nucleated working solid particles with DMA-selected particles. Spherical growth was also assumed in trajectory calculations.

#### 3. Results and Discussion

Sublimation-Condensation System Characterization

Simulations were used to confirm that the designed sublimation-condensation chamber leads to supersaturation of the working solid and are hence presented first. The cylindrical geometry of the sublimation-condensation system enables simulations in an axisymmetric, two-dimensional model of length 0.3 m, and radius of 1.1 cm. Figure 2(a-c) show contour plots of the

normalized temperature, normalized vapor number density, and saturation ratio profiles in the sublimation-condensation system with the working solid TMGN (nominal and fit properties listed in Table 1). The sublimator is simulated at 100°C. A comparison between measured and simulated centerline temperatures is shown in Figure 3 for variable set sublimator temperatures. Consistent with measurements, the temperature increases rapidly and then remains relatively constant through the sublimator. Following the heated section, there is a temperature gradient in the connecting piece between the sublimator and condenser. The core temperature in the condenser is significantly lower than that in the sublimator. As evidenced in Figure 2c, the saturation ratio increases along the axis of the condenser and high levels of supersaturation are achieved (of order 10², using fit vapor pressure parameters, noted subsequently) inside the condenser by saturating and subsequently cooling the working solid vapor-laden flow. Simulations therefore suggest the designed system can yield a high level of supersaturation for working solids needed for condensational growth of low vapor pressure solids.

In describing sublimation-condensation system performance, we refer to the nominal set sublimator temperatures to identify settings, but note that as indicated in Figure 3, for each setting there is a significant spatial-gradient in temperature. Figure 4 displays the inverted size distribution functions with FA as the working solid for variable temperature settings and variable initial sizes of KCl particles introduced. Distribution measurements without passing through sublimation-condensation system are labelled as "initial". As expected, narrow peaks in size distributions are observed in the 30 nm -200 nm diameter range, following selection by the first DMA. We note that because the distribution from the first DMA approximately matches the DMA transfer function and because voltage on the second DMA was systematically stepped and never specifically matched to maximally transmit particles from the first DMA, the peak in size

distributions is not faithfully captured in instances where we bypassed the sublimationcondensation system (Stratmann et al., 1997). Stated differently, for the "initial" distributions, total concentrations may be, and likely are, much higher than inverted values. Percent particle loss values for 50-600 nm particles in the system are also shown in Figure S2 of the supporting information; for all particle diameters, the depositional loss remains below 5%. Increasing the sublimator temperature leads to higher levels of supersaturation and size distributions shift to progressively larger diameters, indicative of increased growth of the working solid material onto particles. We denote the peak positions for variable temperatures (80-100° C) via vertical dashed lines in Figure 4. Almost independent of initial diameter, grown particle diameters approach similar maximum values, ~ 500 nm, making particles optically detectable, and also sufficiently large for concentration enhancement via virtual impactors (Eilts et al., 2023). Growth to a similar diameter, independent of initial diameter, is consistent with condensation kinetics; smaller particles grow faster in diameter and consequently after a sufficient level of condensation, particle size distributions will be independent of the initial size distribution (Friedlander, 2000). At the same time, condensational growth is expected to make size distributions more narrow (Zhang et al., 2012), provided that all particles follow identical saturation ratio and temperature-time histories. However, similar to the results of Attoui (2021) for a sublimation-condensation aerosol generator, we observed distributions become broader due to growth. We attribute this to two potential causes. First, there are spatially-dependent saturation profiles brought about by asymmetric loading of the working fluid in the sublimator (i.e. the working solid is only at the bottom). Particles with trajectories closer to the bottom of the system will be exposed to higher saturation ratios than those traversing the tube near the top. While we attempt to simulate the condensation process, this particular feature is not addressed in simulations, as we utilized an

axisymmetric geometry for simplicity and significantly reduced computational cost. Second, broadening may be brought about by coagulation between homogeneously nucleated particles and the DMA selected particles; we show subsequently that homogeneous nucleation is prevalent when growth occurs, hence the sublimation-condensation system likely leads to growth through both particle-vapor collisions and particle-particle collisions. However, as the number concentration of sublimated vapor molecules and the smallest nucleated particles should vastly exceed the final measured number concentration of homogeneously nucleated particles, it is more likely that collisional growth occurs with sublimated working solid in the vapor phase, or the smallest nucleated working solid particles, which are much smaller than the sampled particles. This influence of coagulational growth with smaller (< 20 nm nanoparticles) on the size distribution width is similar in result to condensational growth; broadening is only expected for coagulation between similarly-sized particles.

We also find that growth yields bimodal mobility-based size distributions. In particular, for larger initial particles, there is a smaller mode than the peak diameter present. This too is anticipated in tandem DMA experiments; the smaller diameter mode is attributable to doubly charged particles transmitted by the DMA (Kim et al., 2005), followed by their growth in the sublimation-condensation system. As we do not correct for multiply charged particles in data inversion, these particles, which are actually larger in initial diameter than the main peak, are interpreted as smaller than their true final diameter. When correcting for multiple charging, their final diameter is found similar to the singly charged particle final diameter, as again, the final diameter is only weakly dependent on the initial DMA selected size.

Similar to Figure 4, Figures 5 and 6 show inverted size distributions with DHB and TMGN, respectively, as the working solids. DHB has a slightly higher melting point (218°C) than that of

FA (170°C). Overall, similar results are obtained with DHB and FA, though with DHB higher temperatures are required to observe growth and, at the same time, we observe little change in size distributions as the sublimator temperature increases from 110°C to 120°C (possibly due to vapor depletion by enhanced homogeneous nucleation). Clearer differences in the extent of growth are observed with TMGN, which is a type of "proton sponge," and a more recently introduced matrix for mass spectrometry for the analysis of low molecular weight compounds (Cao et al., 2011; Qiao & Lissel, 2021). It has a lower melting point (124-128°C) than FA and DHB, and we were able to promote growth with TMGN in the temperature range from 70° C to 90° C. Furthermore, particles grew to noticeably larger diameter with TMGN, larger than 700 nm in many instances with the highest temperature settings. SEM images of particles after TMGN growth are shown in Figure S3 of the supporting information. While grown particles do have several (<5) smaller particles bonded to their surfaces, images show that grown particles have relatively smooth surfaces without evidence of growth solely by agglomeration, i.e. without evidence of growth only by collisions with smaller particles without coalescence. Therefore, if homogeneously nucleated particles do contribute to growth, these particles appear to largely coalesce with sampled particles. Overall, tandem DMA experiments revealed that the sublimation-condensation system successfully leads to growth of particles in the 30 nm -200 nm diameter range to diameters in excess of 500 nm, with the required temperature settings working solid dependent.

Growth onto particles smaller than 7 nm is evidenced in Figure 7, which displays the size distributions of ~7 nm, DMA-selected transferrin monomers without passing through the sublimation-condensation system, and after passing through the system with FA at a condenser temperature of 90° C (and a flow rate of 1.5 SLM). In this case, the grown particles diameters are

in excess of 200 nm, which is not as large as the particles grown from initially > 30 nm particles, but nonetheless demonstrates successful application to sub-10 nm particles.

We also attempt to predict the particle trajectories and particle growth rates in the sublimation-condensation system, assuming vapor condensation is the primary mode of growth and that growth results in spherical particles. Selected particle trajectories based on Brownian Dynamics modeling are shown in Figure 8 for initially 30 nm particles undergoing TMGN condensation at a sublimator temperature of 100°C. As particles migrate through the system, their condensational growth was simulated as described in the supporting information using the condensation rate coefficient model of Gopalakrishnan & Hogan (2011) valid in the transition regime, and with the Kelvin effect (Thomson, 1872) considered. Such growth rate calculations require knowledge of temperature-dependent saturation number density of the working solid,  $n_{Sat}(T)$ .  $n_{Sat}(T)$  yields the spatially-dependent number density, n(T), of the working solid material and saturation  $S = \frac{n(T)}{n_{Sat}(T)}$  from COMSOL simulations of mass transfer.  $n_{Sat}(T)$  was estimated from the Clausius-Clapeyron equation, and hence required the molar enthalpy of vaporization  $\Delta H_{vap}$ , and saturation pressure  $P_{sat}$  for a specific reference temperature. These two parameters were determined by fitting to the experimental results for each working solid, i.e. by forcing the final diameter in trajectory calculations to agree with the mode diameter in experiments. Final fit results for  $\Delta H_{vap}$  and  $P_{sat}$  at 25° C are provided in Table 1. Initial estimates of  $\Delta H_{vap}$  and  $P_{sat}$  were based on the chemical structure database, ChemSpider, which was also used for surface tension data in the condensational growth model (also in Table 1).  $\Delta H_{vap}$  was first adjusted to match the slope of the measured particle growth shown as scatter plots in Figure 8, followed by the adjustments of saturation pressure P<sub>sat</sub> at 25°C to achieve the best agreement with the measurements. Specifically, Figure 9 provides the simulated after-growth diameters of particles

exiting the sublimation-condensation system for the three different test materials FA, DHB and TMGN. The initial diameters of simulated particles (200 in total) followed a triangular mobility distribution following the non-diffusing DMA transfer function, (Knutson & Whitby, 1975) with a midpoint mobility diameter of 100 nm. The particle release position was uniformly sampled along the radial coordinate at the inlet of domain. The mode diameter after growth from experimental measurements for variable initial particle diameters are also plotted in Figure 9, demonstrating that the fit Clausius-Clapeyron equation parameters lead to good agreement between simulations and measurements for all conditions. Fit vapor pressures at 25° C are all of order 10<sup>-4</sup> Pa for all three working solids, necessitating both larger temperature differences and higher saturation ratios for With fit Clausius-Clapeyron equation parameters, we return to the growth results growth. displayed colorimetrically within the trajectories of Figure 8. Independent of trajectory, we observed similar growth for all simulated particles for a given size and system operating condition, again suggesting the broad distributions observed experimentally arise because of the threedimensional nature of the saturation ratio profile. As expected, simulations showed that working solid condensation mainly occurs in the condenser region and diameter change rate reaches the maximum in the connecting section. As in the experiments, simulation results also suggest that the initial particle diameter has minimal influence on the final particle diameter.

#### Homogenous Nucleation Characterization

Tandem DMA experiments and accompanying modeling demonstrate that the sublimation-condensation system does enable condensation onto particles of low vapor pressure solids. However, these results do not quantify the extent of homogenous nucleation, and SEM images do suggest collisional growth between sampled particles and smaller, presumably working solid

particles does occur. Furthermore, while average particle diameters after growth can be explained entirely by fitting a model assuming growth occurs via condensation, we remark that this does not rule out non-negligible influences of coagulational growth of homogeneously nucleation particles. To address the unanswered issue of homogeneous nucleation, we measured the size distributions for nucleated working solid particles in the absence of KCl particles, with results shown in Figure 10. In all circumstances, significant homogenous nucleation is observed at temperature settings equal to and above 80° C, i.e. there are working solid-only particles are present. At the highest setting temperature of 100°C, homogenous nucleation yields larger number concentrations, and logarithmic size distributions above 2×10<sup>5</sup> cm<sup>-3</sup> for all three test materials. Although the majority of the homogeneously nucleated particles are smaller than 300 nm in diameter for most examined conditions, there is a non-zero concentration of particles above 300 nm in diameter. In a highly related research effort, Attoui (2021) examined the ability of a laminar flow evaporationcondensation system with low vapor pressure compounds to produce strictly singly-charged submicrometer to supermicrometer particles as test particles for aerosol experiments. In this system, singly-charged corona discharge generated ions (sub-nanometer scale in size) were injected into the system and facilitated ion-induced nucleation, hence charging was accomplished on vapor phase species first, following by particle growth. Homogeneous nucleation also occurred in parallel with ion-induced nucleation, with similar particle size distributions to those presented here for homogeneous nucleation. As in Attoui (2021), the homogeneously nucleated particles in this study are electrically neutral, and hence can be removed from the flow system by DMA selection, i.e. by using a DMA-sublimation-condensation-DMA system, if and when desired. This would need to be the case for application in single particle mass spectrometry, for example, but for more generable particle concentration or collection, may not be necessary. In both studies,

growth of particles via coagulation of homogeneously nucleated particles with sampled particles (here) or ion-induced nucleation formed particles cannot be dismissed as a growth mechanism. However, this too, has little bearing on the actual performance of the systems developed; in both cases the end result is grown particles to a target mobility diameter for eventual sampling or analysis. Of future interest would be aerodynamic diameter determination or mass measurement to confirm spherical growth of particles, and to better understand the potential interplay between condensational growth, and coagulational growth (truly agglomeration, if non-spherical particles result) in sublimation systems.

#### **Conclusions**

A laminar flow sublimation-condensation system for low vapor pressure solid growth onto particles has been developed and applied to examine how three different matrix materials used in MALDI-MS function as working solids (FA, DHB and TMGN). The performance of the system has been characterized by size distributions from tandem DMA measurements of heterogeneously grown particles and single DMA measurements of homogeneous nucleation of vapor molecules. The results show that the sublimation-condensation system successfully leads to growth onto particles in the 30 nm – 200 nm diameter range to diameters above 500 nm for all three examined solids with the required material-dependent temperature settings. Sub-10 nm particle growth (onto transferrin monomers) to diameters >100 nm was also achieved with FA. We find that growth with TMGN yields the most significant increases of particle diameters at lower temperatures. The extent of heterogeneous growth and homogenous nucleation both increase with increasing sublimator set temperatures, which requires further system refinement to increase heterogeneous growth without the incidence of homogeneous nucleation.

The data presented in this study follow a similar research thread to the recent studies of Attoui (2021) on utilizing low vapor pressure material growth for aerosol standards, and of Collings et al. (2014) and Kupper et al. (2020), who sought to develop aerosol condensation systems functioning above 100° C (towards exhaust emission detection). Each of these studies makes use of standard aerosol growth techniques operated outside of traditional operating conditions and with non-traditional working materials. Collectively, this study and these studies find that by modulating working materials and operating temperatures, it is possible to regulate the extent of nanoparticle growth and the extent of homogeneous nucleation in aerosol systems.

## **Supporting Information**

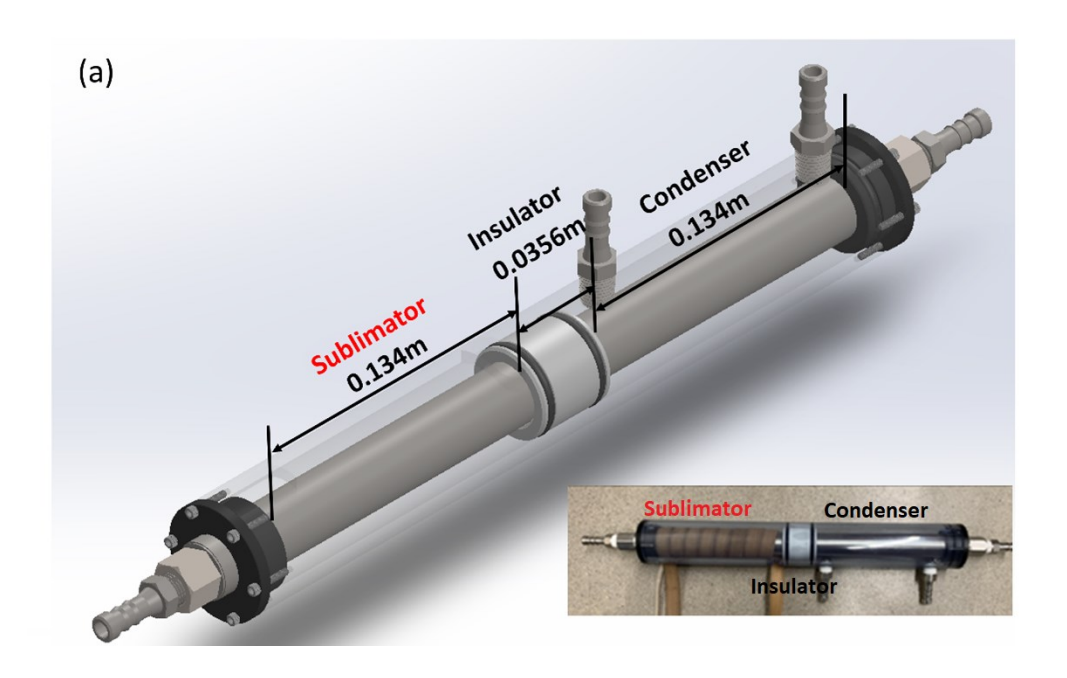
A description of simulations used to examine heat and mass transfer in the sublimationcondensation system, a description of particle trajectory and condensational growth simulations, particle transmission efficiency measurements in the system, and particle SEM images are available online.

# Acknowledgements

This work was supported by US National Science Foundation Grants GEO-2035847 and GEO-2035870. Scanning electron microscopy was performed at the University of Minnesota Characterization Facility (CharFac) which receives partial support from the NSF through the MRSEC (Award Number DMR-2011401) and the NNCI (Award Number ECCS-2025124) programs.

**Table 1.** A summary of the relevant properties of working solid materials. FA: Ferulic Acid; 2,4-DHB: 2,4-dihydroxybenzoic acid; TMGN: 1,8-bis(tetramethylguanidino)naphthalene. Fit saturation vapor pressures at 25° C at the fit heat of vaporization are determined from comparison of measured and modeled final particle diameters in sublimation-condensation experiments. The model assumes growth is entirely due to condensation, and leads to spherical particles.

			Chemspider			Fit	
	Molar Mass (g/mol)	Density (kg/m³)	Surface Tension (dyne/cm)	$\Delta H_{vap}$ (kJ/mol)	<i>P<sub>sat</sub></i> (Pa) @ 25°C	$\Delta H_{vap}$ (kJ/mol)	<i>P<sub>sat</sub></i> (Pa) @ 25°C
FA	194	1320	56.2	65.3	3.65x10 <sup>-3</sup>	62.3	2.20x10 <sup>-4</sup>
2,4-DHB	154	1600	84.3	70.4	3.01x10 <sup>-3</sup>	60	2.00 x10 <sup>-4</sup>
TMGN	354	1000	34.7	73.5	8.33 x10 <sup>-5</sup>	73.5	1.40 x10 <sup>-4</sup>



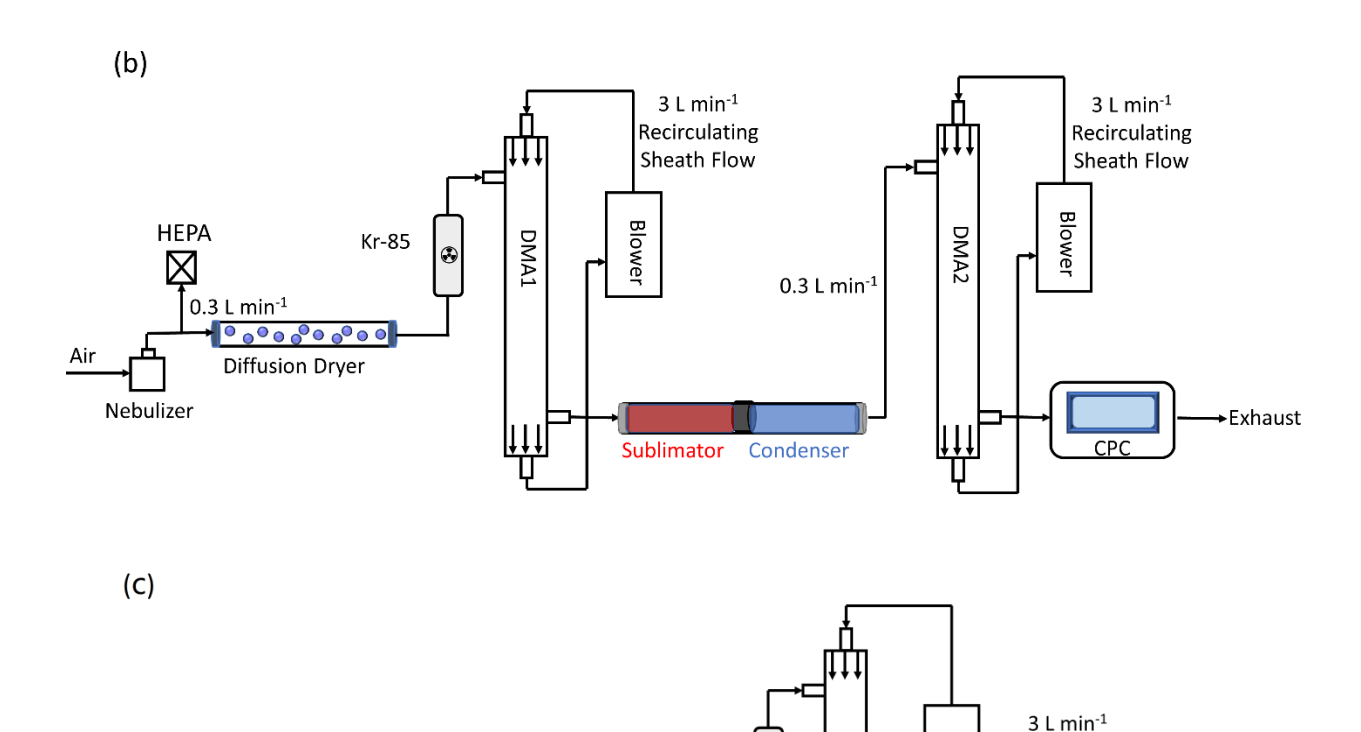


**Figure 1.** An isometric view and photograph (inset) of the laminar flow sublimation-condensation system developed for growth of particles (a). A schematic diagram of the tandem differential mobility analyzer system used to evaluate particle growth with the sublimation-condensation system (b). A schematic diagram of the differential mobility particle sizer system measuring the size distribution of homogenous nucleation of working solid vapor molecules (c).

Kr-85

0.3 L min<sup>-1</sup>

Condenser

**Sublimator** 

HEPA

Room Air -

DMA

Recirculating

Sheath Flow

**►**Exhaust

0.3 L min<sup>-1</sup>

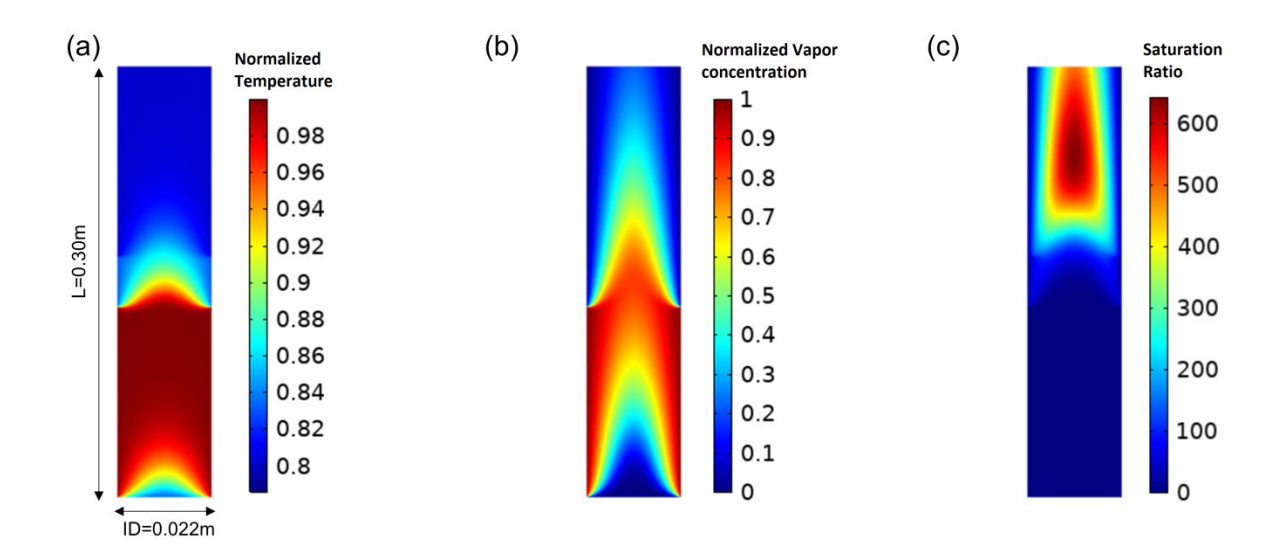


**Figure 2.** Heat maps of the normalized temperature with respect to the maximum observed in simulations (a), normalized vapor concentration (b), and saturation ratio (c) resulting from COMSOL simulations of the sublimation-condensation system. Saturation ratio plots apply for the material 1,8-bis(tetramethylguanidino)naphthalene (TMGN) with a sublimator temperature of 100°C and the best-fit saturation vapor pressure parameters in Table 1.

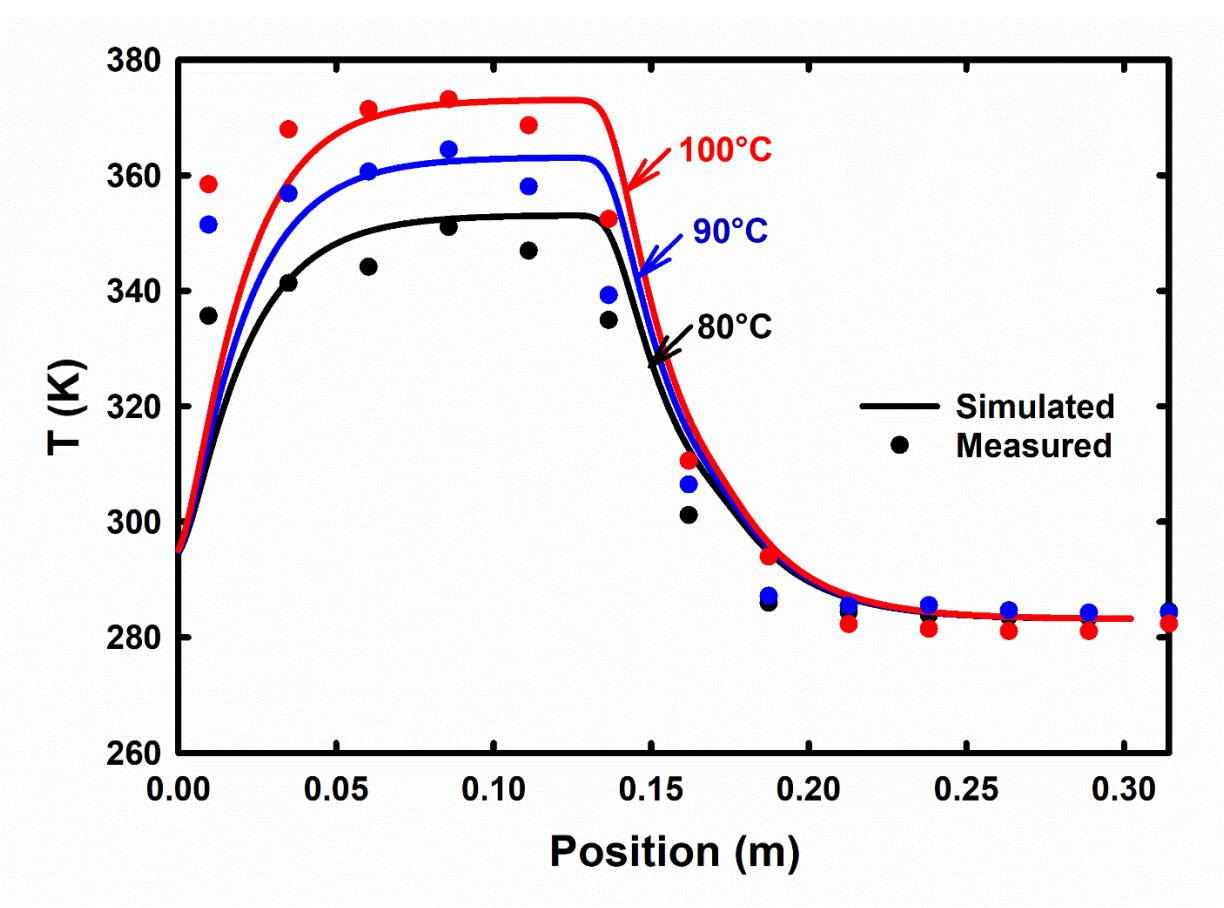


**Figure 3.** The centerline temperature in the sublimation-condensation system as determined from measurements and COMSOL simulations. 80°C in black; 90°C in blue; 100°C in red.

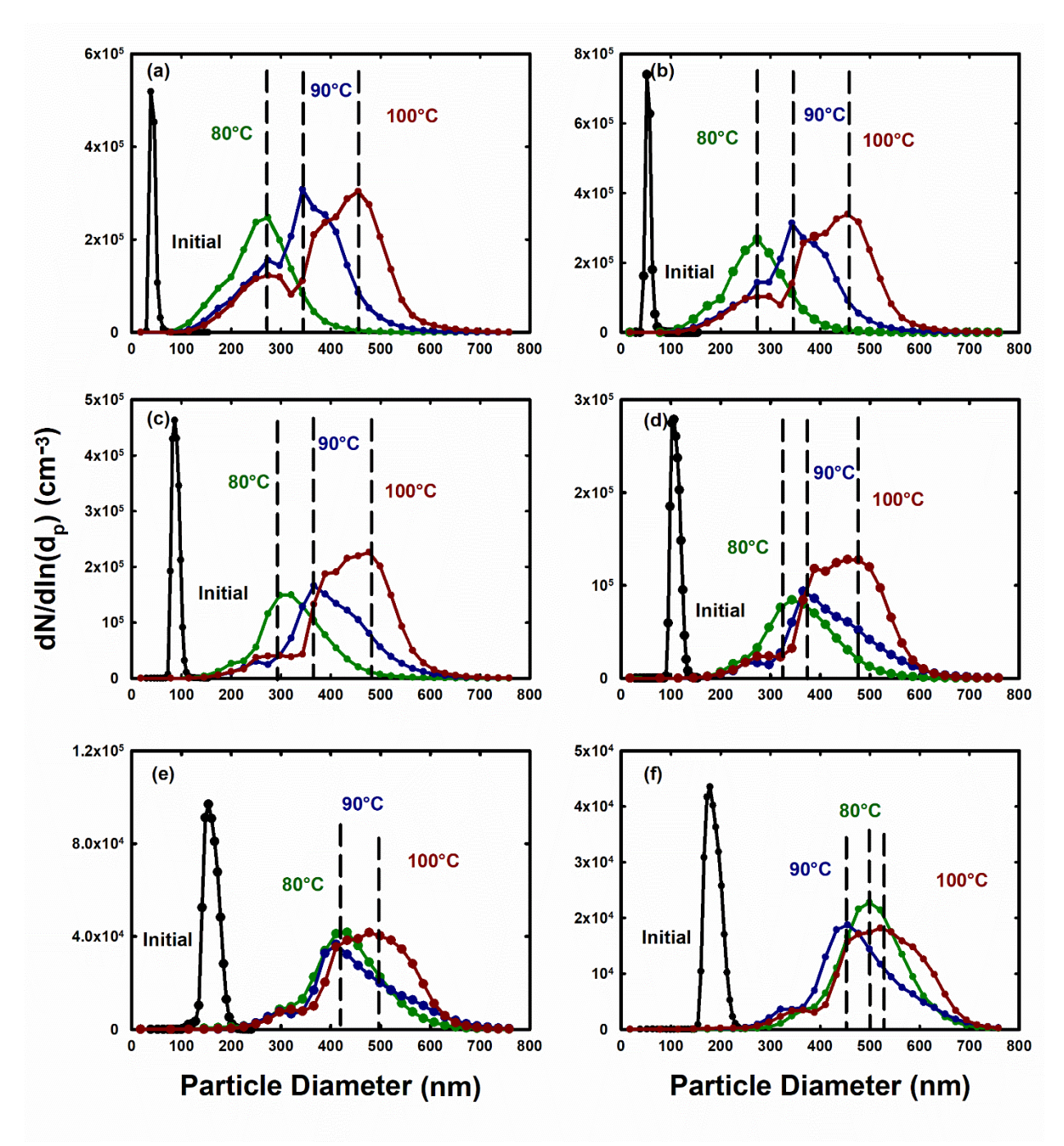


**Figure 4.** Size distributions from tandem differential mobility analyzer experiments with ferulic acid (FA) as the condensing solid for 38 nm (a), 52 nm (b), 82 nm (c), 102 nm (d), 148 nm (e), and 196 nm (f) KCl particles. Labelled temperatures denote the set sublimator temperature. "Initial" corresponds to the size distribution bypassing the sublimation-condensation system. 80°C in green; 90°C in blue; 100°C in red.

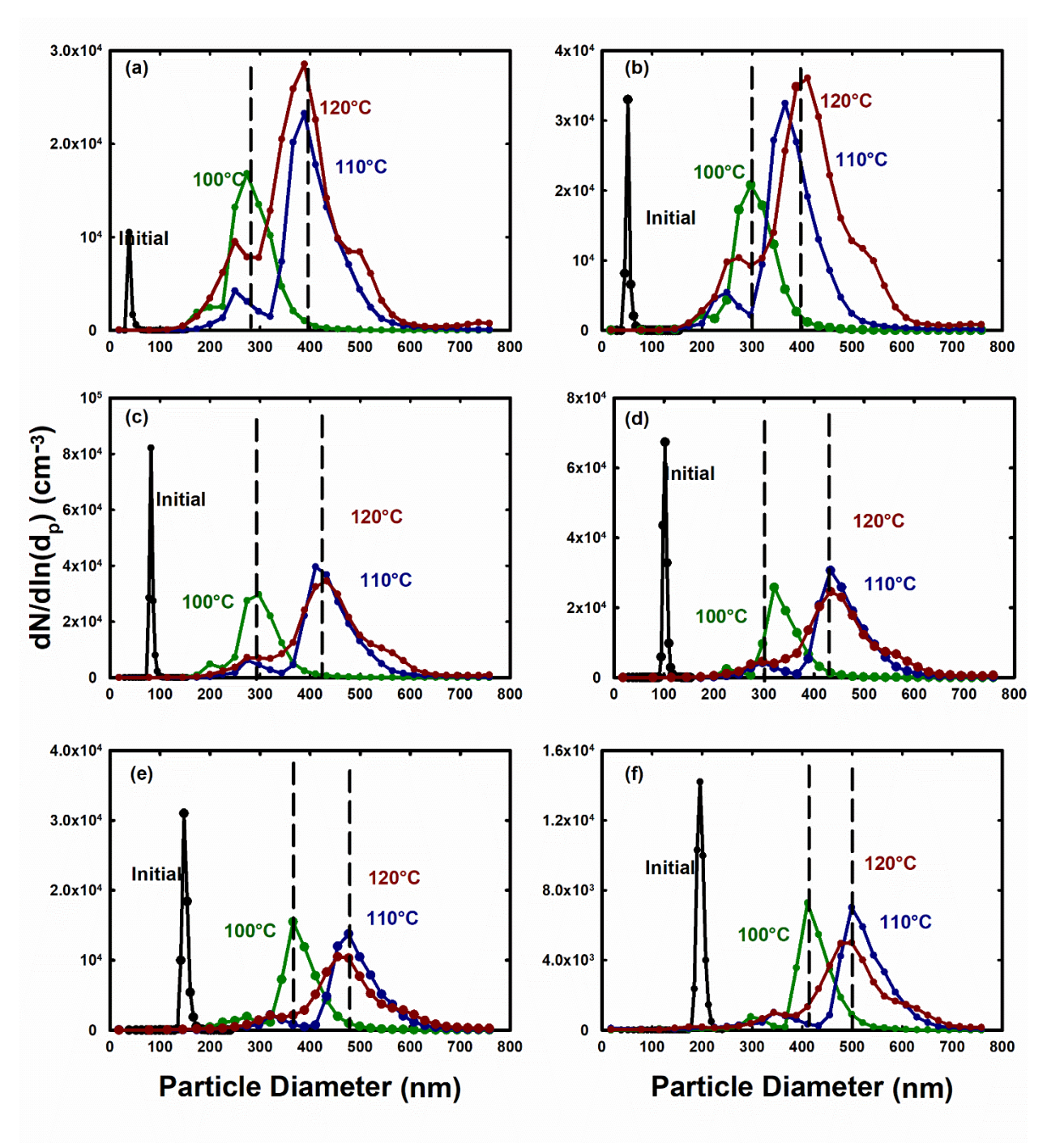


**Figure 5.** Size distributions from tandem differential mobility analyzer experiments with 2,4-dihydroxybenzoic acid (DHB) as the condensing solid for 38 nm (a), 52 nm (b), 82 nm (c), 102 nm (d), 148 nm (e), and 196 nm (f) KCl particles. Labelled temperatures denote the set sublimator temperature. "Initial" corresponds to the size distribution bypassing the sublimation-condensation system. 100°C in green; 110°C in blue; 120°C in red.

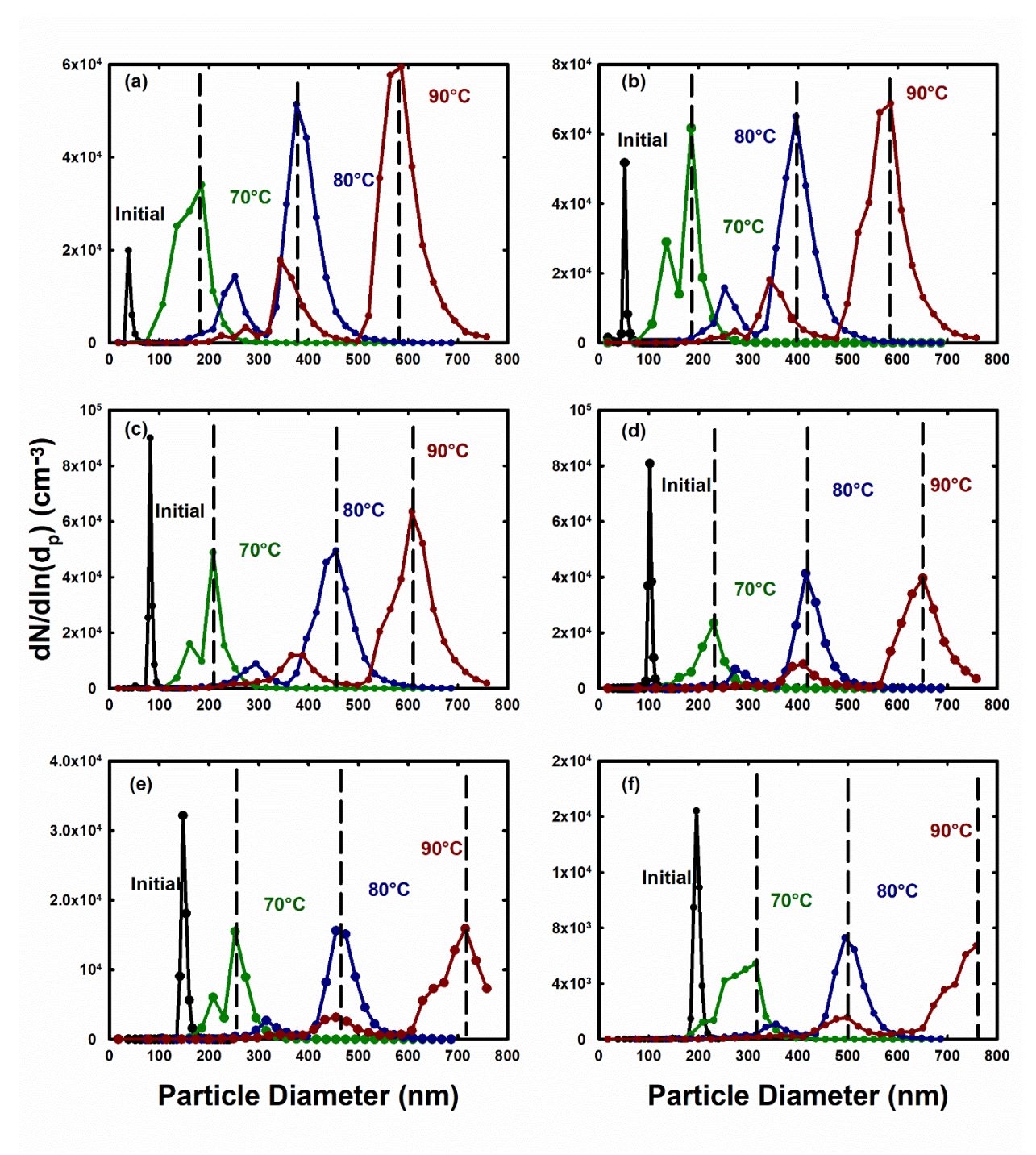


**Figure 6.** Size distributions from tandem differential mobility analyzer experiments 1,8-bis(tetramethylguanidino)naphthalene (TMGN) as the condensing solid for 38 nm (a), 52 nm (b), 82 nm (c), 102 nm (d), 148 nm (e), and 196 nm (f) KCl particles. Labelled temperatures denote the set sublimator temperature. "Initial" corresponds to the size distribution bypassing the sublimation-condensation system. 70°C in green; 80°C in blue; 90°C in red.

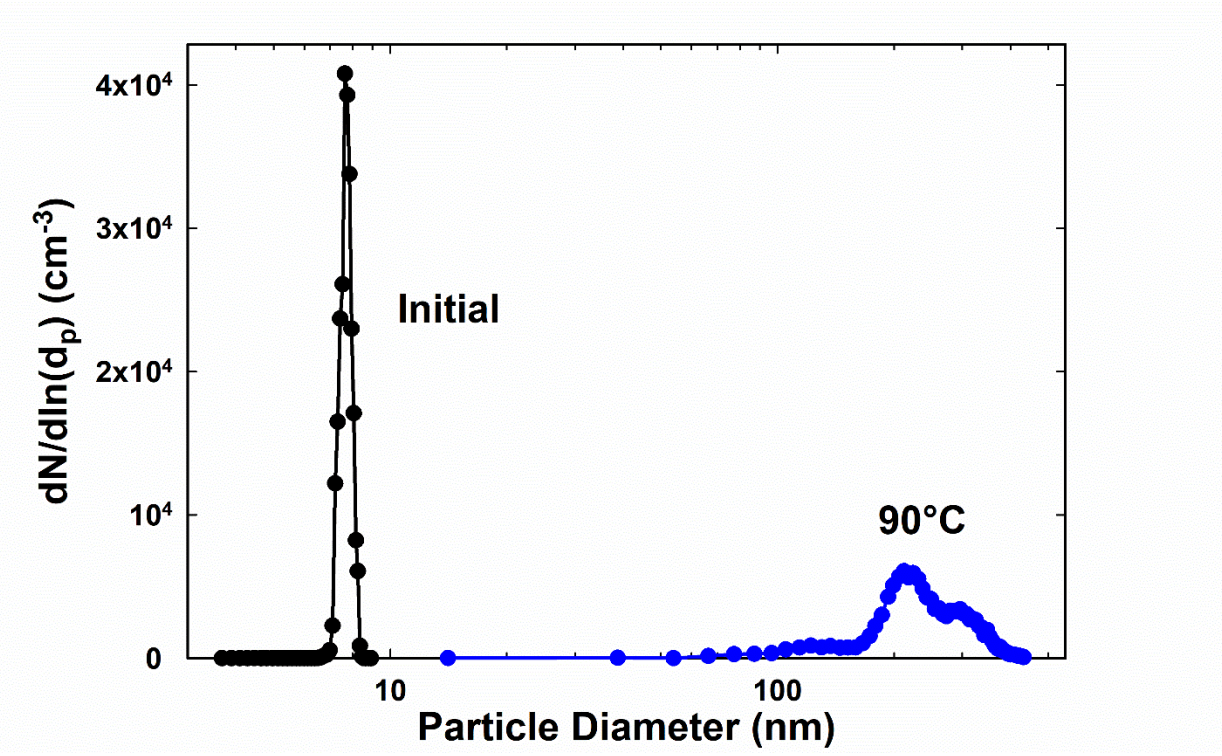


**Figure 7.** Size distributions of mobility selected transferrin monomers (nominally at 7 nm mobility diameter) initially, and after passing through the sublimation-condensation system at a flow rate of 1.5 SLM, and ferulic acid (FA) as the condensing solid.

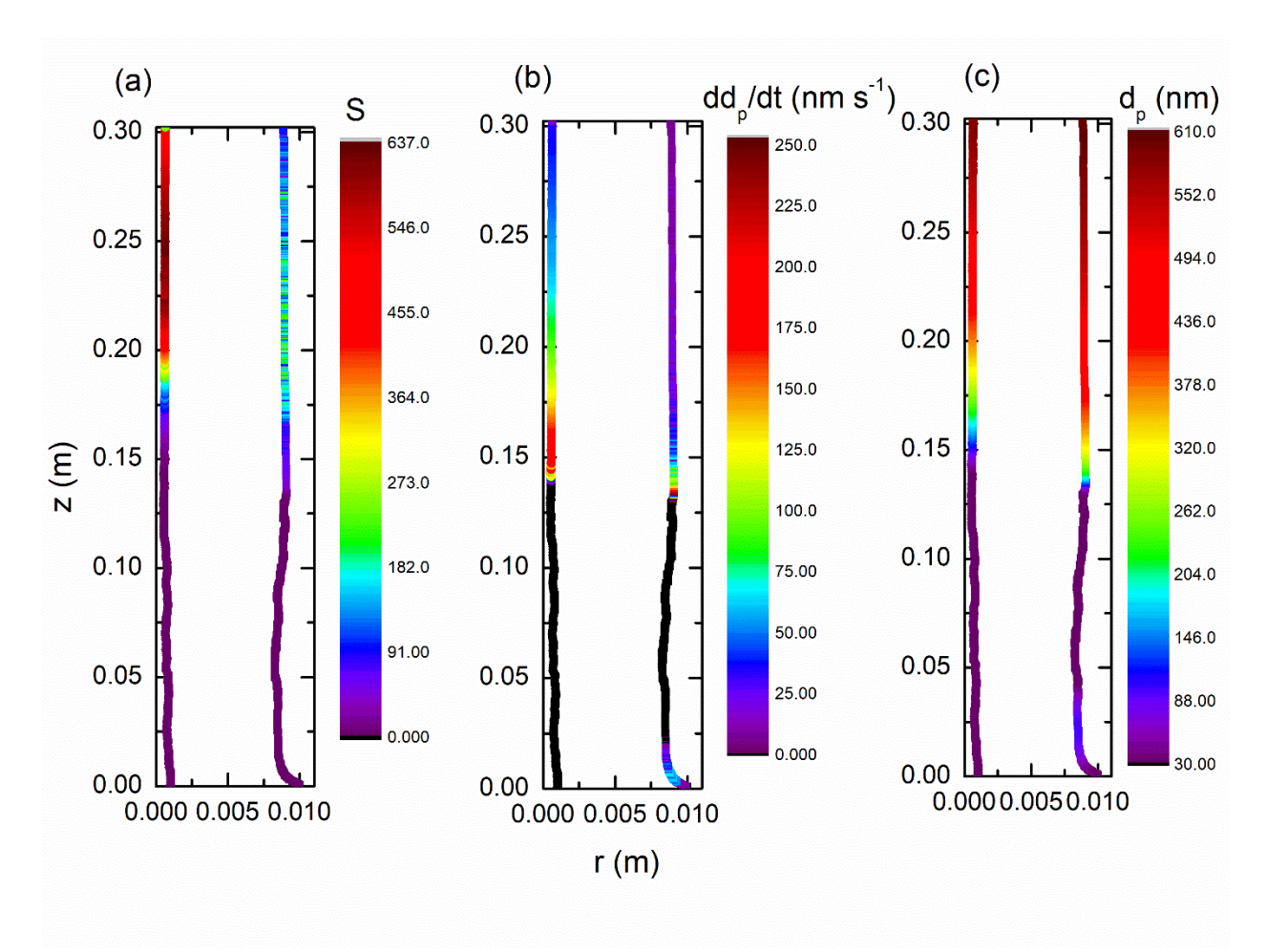


**Figure 8.** Sample trajectories from simulations of initially 30 nm particles released at radial axis  $r = 10^{-3}$  m and  $10^{-2}$  m in the sublimation-condensation system, assuming growth occurs solely by condensation. Color contours denote the local saturation ratio (a), time rate of change of particle diameter (b), and particle diameter (c). Simulations correspond to 1,8-bis(tetramethylguanidino)naphthalene (TMGN) as the condensing solid and a sublimator temperature of  $100^{\circ}$ C.

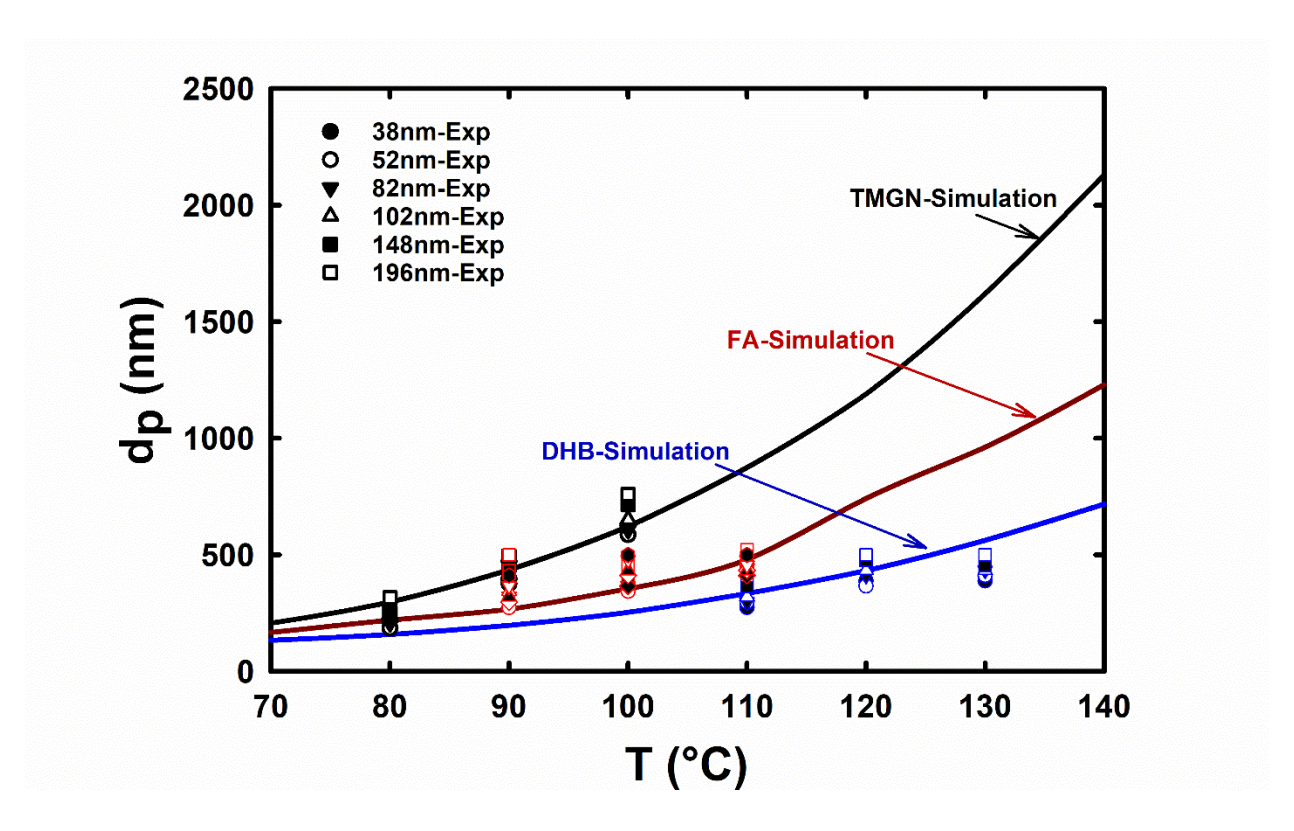


**Figure 9.** A comparison of measured particle diameters at the condenser outlet (mode diameter in distributions) compared to simulations with best-fit Clausius-Clapeyron parameters for the three tested working solids. Simulations apply to 100 nm particles transmitted by a DMA, although the initial particle diameter has little influence on the results. All results apply to spherical particle growth with condensation only considered as the growth mechanism.

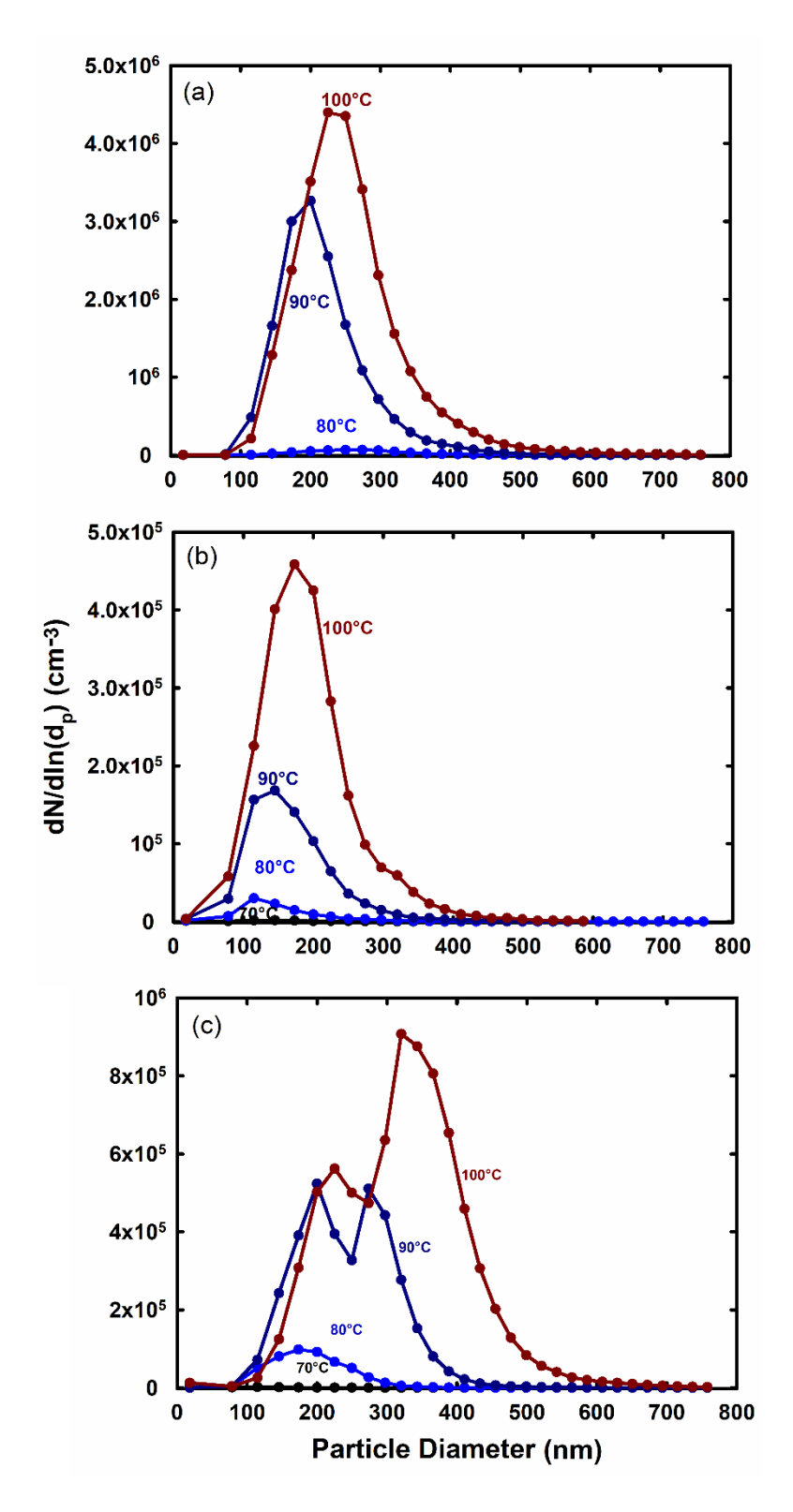


**Figure 10.** Inverted size distributions for solid particles in single differential mobility analyzer experiments, indicating the extent of homogenous nucleation in the sublimation-condensation system. Ferulic acid (FA) (a), 2,4-dihydroxybenzoic acid (DHB) (b), 1,8-bis(tetramethylguanidino)naphthalene (TMGN) (c).

#### References

- Agarwal, J. K., & Sem, G. J. (1980). Continuous flow, single-particle-counting condensation nucleus counter. *Journal of Aerosol Science*, 11(4), 343-357.
- Attoui, M. (2021). Ion induced nucleation based-generator of strictly singly charged (solid liquid) polydisperse particles up to 1 μm. *Journal of Aerosol Science*, 153, 105732.
- Boies, A. M., Lei, P., Calder, S., & Girshick, S. L. (2011). Gas-phase production of gold-decorated silica nanoparticles. *Nanotechnology*, 22(31), 315603.
- Bricard, J., Delattre, P., Madelaine, G., & Pourprix, M. (1976). Detection of Ultra-Fine Particles by Means of a Continuous Flux Condensation Nuclei Counter. In B. Y. H. Liu (Ed.), *Fine Particles: Aerosol Generation, Measurement, Sampling, and Analysis* (pp. 565-580). New York, NY: Academic Press, New York.
- Cao, D., Wang, Z., Han, C., Cui, L., Hu, M., Wu, J., . . . Kang, Y. (2011). Quantitative detection of trace perfluorinated compounds in environmental water samples by Matrix-assisted Laser Desorption/Ionization-Time of Flight Mass Spectrometry with 1,8-bis(tetramethylguanidino)-naphthalene as matrix. *Talanta*, 85(1), 345-352.
- Collings, N., Rongchai, K., & Symonds, J. P. R. (2014). A condensation particle counter insensitive to volatile particles. *Journal of Aerosol Science*, 73, 27-38.
- Dixkens, J., & Fissan, H. (1999). Development of an Electrostatic Precipitator for Off-Line Particle Analysis. *Aerosol Science and Technology*, 30(5), 438-453.
- Eilts, S. M., Tamadate, T., Relling, M. E., Marabella, I. A., Hogan, C. J., & Olson, B. A. (2023). Virtual impaction in compressible flows with pressure recovery. *Journal of Aerosol Science*, 167, 106076.
- Fei, X., Wei, G., & Murray, K. K. (1996). Aerosol MALDI with a Reflectron Time-of-Flight Mass Spectrometer. *Analytical Chemistry*, 68(7), 1143-1147.
- Friedlander, S. K. (2000). Smoke, Dust, and Haze. New York: Oxford University Press.
- Gamero-Castaño, M., & Fernández de la Mora, J. (2000). A Condensation Nucleus Counter (CNC) Sensitive to Singly Charged Sub-Nanometer Particles. *Journal of Aerosol Science*, 31(7), 757-772.
- Gopalakrishnan, R., & Hogan, C. J. (2011). Determination of the Transition Regime Collision Kernel from Mean First Passage Times. *Aerosol Science and Technology*, 45(12), 1499-1509.
- Hao, W., Stolzenburg, M., Attoui, M., Zhang, J., & Wang, Y. (2021). Optimizing the activation efficiency of sub-3 nm particles in a laminar flow condensation particle counter: Model simulation. *Journal of Aerosol Science*, 158, 105841.
- Harris, W. A., Reilly, P. T. A., & Whitten, W. B. (2005). MALDI of Individual Biomolecule-Containing Airborne Particles in an Ion Trap Mass Spectrometer. *Analytical Chemistry*, 77(13), 4042-4050.
- Harris, W. A., Reilly, P. T. A., & Whitten, W. B. (2006). Aerosol MALDI of peptides and proteins in an ion trap mass spectrometer: Trapping, resolution and signal-to-noise. *International Journal of Mass Spectrometry*, 258(1), 113-119.
- Hering, S. V., Stolzenburg, M. R., Quant, F. R., Oberreit, D. R., & Keady, P. B. (2005). A Laminar-Flow, Water-Based Condensation Particle Counter (WCPC). *Aerosol Science and Technology*, 39(7), 659-672.

- Iida, K., Stolzenburg, M. R., & McMurry, P. H. (2009). Effect of Working Fluid on Sub-2 nm Particle Detection with a Laminar Flow Ultrafine Condensation Particle Counter. *Aerosol Science and Technology*, 43(1), 81-96.
- Jackson, S. N., Mishra, S., & Murray, K. K. (2004). On-line laser desorption/ionization mass spectrometry of matrix-coated aerosols. [https://doi.org/10.1002/rcm.1590]. *Rapid Communications in Mass Spectrometry*, 18(18), 2041-2045.
- Jackson, S. N., & Murray, K. K. (2002). Matrix Addition by Condensation for Matrix-Assisted Laser Desorption/Ionization of Collected Aerosol Particles. *Analytical Chemistry*, 74(18), 4841-4844.
- Jeon, S., Oberreit, D. R., Van Schooneveld, G., & Hogan, C. J. (2016). Liquid Nebulization—Ion Mobility Spectrometry Based Quantification of Nanoparticle—Protein Conjugate Formation. *Analytical Chemistry*, 88(15), 7667-7674.
- Jiang, J., Chen, M., Kuang, C., Attoui, M., & McMurry, P. H. (2011). Electrical Mobility Spectrometer Using a Diethylene Glycol Condensation Particle Counter for Measurement of Aerosol Size Distributions Down to 1 nm. *Aerosol Science and Technology*, 45(4), 510-521.
- Johnson, T. J., Nishida, R. T., Irwin, M., Symonds, J. P. R., Olfert, J. S., & Boies, A. M. (2020). Measuring the bipolar charge distribution of nanoparticles: Review of methodologies and development using the Aerodynamic Aerosol Classifier. *Journal of Aerosol Science*, 143, 105526.
- Kim, S., Jaques, P. A., Chang, M., Froines, J. R., & Sioutas, C. (2001). Versatile aerosol concentration enrichment system (VACES) for simultaneous in vivo and in vitro evaluation of toxic effects of ultrafine, fine and coarse ambient particles Part I: Development and laboratory characterization. *Journal of Aerosol Science*, 32(11), 1281-1297.
- Kim, S. H., Woo, K. S., Liu, B. Y. H., & Zachariah, M. R. (2005). Method of measuring charge distribution of nanosized aerosols. *Journal of Colloid and Interface Science*, 282(1), 46-57.
- Knutson, E. O., & Whitby, K. T. (1975). Aerosol classification by electric mobility: apparatus, theory, and applications. *Journal of Aerosol Science*, 6(6), 443-451.
- Kreisberg, N. M., Spielman, S. R., Eiguren-Fernandez, A., Hering, S. V., Lawler, M. J., Draper, D. C., & Smith, J. N. (2018). Water condensation-based nanoparticle charging system: Physical and chemical characterization. *Aerosol Science and Technology*, 52(10), 1167-1177.
- Kupper, M., Kraft, M., Boies, A., & Bergmann, A. (2020). High-temperature condensation particle counter using a systematically selected dedicated working fluid for automotive applications. *Aerosol Science and Technology*, 54(4), 381-395.
- Lee, J., Clowers, B. T., & Hogan, C. J. (2022). Condensable Vapor Sorption by Low Charge State Protein Ions. *Analytical Chemistry*, *94*, 7050–7059.
- Li, L., & Gopalakrishnan, R. (2021). An experimentally validated model of diffusion charging of arbitrary shaped aerosol particles. *Journal of Aerosol Science*, 151, 105678.
- McJimpsey, E. L., Jackson, W. M., Lebrilla, C. B., Tobias, H., Bogan, M. J., Gard, E. E., . . . Steele, P. T. (2008). Parameters contributing to efficient ion generation in aerosol MALDI mass spectrometry. *Journal of the American Society for Mass Spectrometry*, 19(3), 315-324.
- McMurry, P. H. (2000). The History of Condensation Nucleus Counters. *Aerosol Science and Technology*, 33(4), 297-322.

- Okuyama, K., Kousaka, Y., & Motouchi, T. (1984). Condensational Growth of Ultrafine Aerosol Particles in a New Particle Size Magnifier. *Aerosol Science and Technology*, *3*(4), 353-366.
- Perry, D. G., & Smaldone, G. C. (1985). Factors affecting aerosol production from a modified sinclair-la mer aerosol generator. *Journal of Aerosol Science*, 16(5), 427-436.
- Post, P., Wurlitzer, L., Maus-Friedrichs, W., & Weber, A. P. (2018). Characterization and Applications of Nanoparticles Modified in-Flight with Silica or Silica-Organic Coatings. *Nanomaterials*, 8(7). Retrieved from doi:10.3390/nano8070530
- Qiao, Y., Li, L., Chen, J., Yang, S., & Hogan, C. J. (2022). Mobility analysis of nanocluster formation and growth from titanium tetraisopropoxide in a flow tube reactor. *Journal of Aerosol Science*, 163, 105981.
- Qiao, Z., & Lissel, F. (2021). MALDI Matrices for the Analysis of Low Molecular Weight Compounds: Rational Design, Challenges and Perspectives. [https://doi.org/10.1002/asia.202100044]. *Chemistry An Asian Journal*, 16(8), 868-878.
- Rader, D. J., & McMurry, P. H. (1986). Application of the tandem differential mobility analyzer to studies of droplet growth or evaporation. *Journal of Aerosol Science*, 17(5), 771-787.
- Rörup, B., Scholz, W., Dada, L., Leiminger, M., Baalbaki, R., Hansel, A., . . . Lehtipalo, K. (2022). Activation of sub-3 nm organic particles in the particle size magnifier using humid and dry conditions. *Journal of Aerosol Science*, 161, 105945.
- Sinclair, D., & La Mer, V. K. (1949). Light Scattering as a Measure of Particle Size in Aerosols. The Production of Monodisperse Aerosols. *Chemical reviews*, 44(2), 245-267.
- Stolzenburg, M. R., & McMurry, P. H. (1991). An Ultrafine Aerosol Condensation Nucleus Counter. *Aerosol Science and Technology*, 14(1), 48-65.
- Stowers, M. A., van Wuijckhuijse, A. L., Marijnissen, J. C. M., Scarlett, B., van Baar, B. L. M., & Kientz, C. E. (2000). Application of matrix-assisted laser desorption/ionization to online aerosol time-of-flight mass spectrometry. [https://doi.org/10.1002/(SICI)1097-0231(20000530)14:10<829::AID-RCM951>3.0.CO;2-3]. Rapid Communications in Mass Spectrometry, 14(10), 829-833.
- Stratmann, F., Kauffeldt, T., Hummes, D., & Fissan, H. (1997). Differential Electrical Mobility Analysis: A Theoretical Study. *Aerosol Science and Technology*, 26(4), 368-383.
- Suh, J., Han, B., Seong Kim, D., & Choi, M. (2005). A method for enhanced charging of nanoparticles via condensation magnification. *Journal of Aerosol Science*, 36(10), 1183-1193.
- Suresh, V., Li, L., Redmond Go Felipe, J., & Gopalakrishnan, R. (2021). Modeling nanoparticle charge distribution in the afterglow of non-thermal plasmas and comparison with measurements. *Journal of Physics D: Applied Physics*, 54(27), 275205.
- Thomas, J. M., Chen, X., Maißer, A., & Hogan, C. J. (2018). Differential heat and mass transfer rate influences on the activation efficiency of laminar flow condensation particle counters. *International Journal of Heat and Mass Transfer*, 127, 740-750.
- Thomson, W. (1872). 4. On the Equilibrium of Vapour at a Curved Surface of Liquid. *Proceedings of the Royal Society of Edinburgh*, 7, 63-68.
- van Wuijckhuijse, A. L., Stowers, M. A., Kleefsman, W. A., van Baar, B. L. M., Kientz, C. E., & Marijnissen, J. C. M. (2005). Matrix-assisted laser desorption/ionisation aerosol time-of-flight mass spectrometry for the analysis of bioaerosols: development of a fast detector for airborne biological pathogens. *Journal of Aerosol Science*, 36(5), 677-687.

- Xia, W.-w., Ti, R.-f., Zhang, Z.-I., Zheng, H.-y., & Fang, L. (2010). Influence Factors on Particle Growth for On-line Aerosol Matrix-assisted Laser Desorption/Ionization Time-of-flight Mass Spectrometry. *Chinese Journal of Chemical Physics*, 23(3), 269-273.
- Zhang, X., Pandis, S. N., & Seinfeld, J. H. (2012). Diffusion-Limited Versus Quasi-Equilibrium Aerosol Growth. *Aerosol Science and Technology*, 46(8), 874-885.
- Zhou, L., Zhu, Y., Guo, X., Zhao, W., Zheng, H., Gu, X., . . . Zhang, W. (2006). On-line matrix addition for detecting aerosol particles. *Science in China Series G*, 49(2), 187-194.